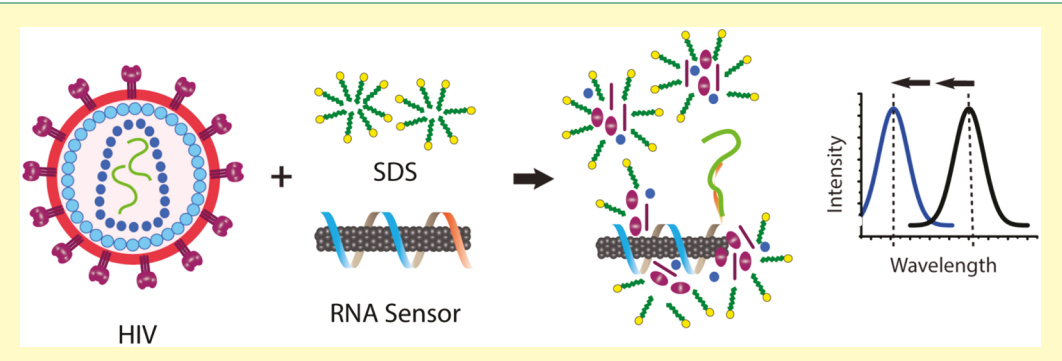


# HIV Detection via a Carbon Nanotube RNA Sensor

Jackson D. Harvey, †,‡6 Hanan A. Baker, †,‡6 Michael V. Ortiz,† Alex Kentsis,†,‡ and Daniel A. Heller\*,†,‡6

Supporting Information



ABSTRACT: Viral illnesses remain a significant concern in global health. Rapid and quantitative early detection of viral oligonucleotides without the need for purification, amplification, or labeling would be valuable in guiding successful treatment strategies. Single-walled carbon nanotube-based sensors recently demonstrated optical detection of small, free oligonucleotides in biofluids and in vivo, although proteins diminished sensitivity. Here, we discovered an unexpected phenomenon wherein the carbon nanotube optical response to nucleic acids can be enhanced by denatured proteins. Mechanistic studies found that hydrophobic patches of the denatured protein chain interact with the freed nanotube surface after hybridization, resulting in enhanced shifting of the nanotube emission. We employed this mechanism to detect an intact HIV in serum, resulting in specific responses within minutes. This work portends a route toward point-of-care optical detection of viruses or other nucleic acid-based analytes.

KEYWORDS: biosensors, nanosensors, human immunodeficiency virus, AIDS, fluorescence

espite a widespread effort to combat the spread of human immunodeficiency virus (HIV), recent data from the World Health Organization estimates that there are 36.9 million people globally living with HIV, but only 59% percent of them are receiving much needed antiretroviral treatment. In many regions with a high incidence of HIV, such as sub-Saharan Africa, the limited access to healthcare resources likely hinders the implementation of effective diagnosis and treatment strategies. One strategy to overcome these challenges is to use rapid, point-of-care diagnostics, which have been shown to increase the number of patients who know their infection status. Although antibody-based testing is currently used in this setting, the false-positive and false-negative rates remain a significant limitation.

As an alternative biomarker, cell-free oligonucleotides in biofluids such as serum offer the potential to diagnose, monitor, and stratify disease states based on specific expression patterns, changes, or mutations.<sup>2-4</sup> Indeed, realizing such potential has been the subject of recent work focusing on "liquid biopsies",5 which aims to use accessible biomarkers to complement or even obviate the need for an invasive, traditional biopsy. While the focus of cell-free oligonucleotide detection has been for cancer, many other diseases of interest

also show specific expression patterns of oligonucleotides.<sup>6</sup> Specifically, the measurement of exogenous DNA and RNA strands found in viruses is a promising method for rapid diagnosis of infectious diseases.7 Rapid, quantitative detection of viral oligonucleotides without the need for purification, amplification, or labeling of the oligonucleotide could help diagnose infections before symptoms appear, monitor the course of the disease, and also characterize viral subtypes and clades.8 A simple point-of-care option would therefore be especially valuable in developing countries prone to infectious disease outbreak, especially HIV. Because the viral genome is typically sequestered inside a protein capsid and in some cases an additional lipid bilayer, a point-of-care sensor would have to be compatible with lysing conditions to liberate the viral oligonucleotides. In addressing the need for such point-of-care options, diverse solutions based on nanomaterials are being developed, which have recently been reviewed elsewhere.

Single-walled carbon nanotubes are one class of nanomaterials capable of optical transduction of binding events via

Received: January 4, 2019 Accepted: April 23, 2019 Published: May 6, 2019

<sup>&</sup>lt;sup>†</sup>Memorial Sloan Kettering Cancer Center, New York, New York 10065, United States \*Weill Cornell Medical College, New York, New York 10065, United States

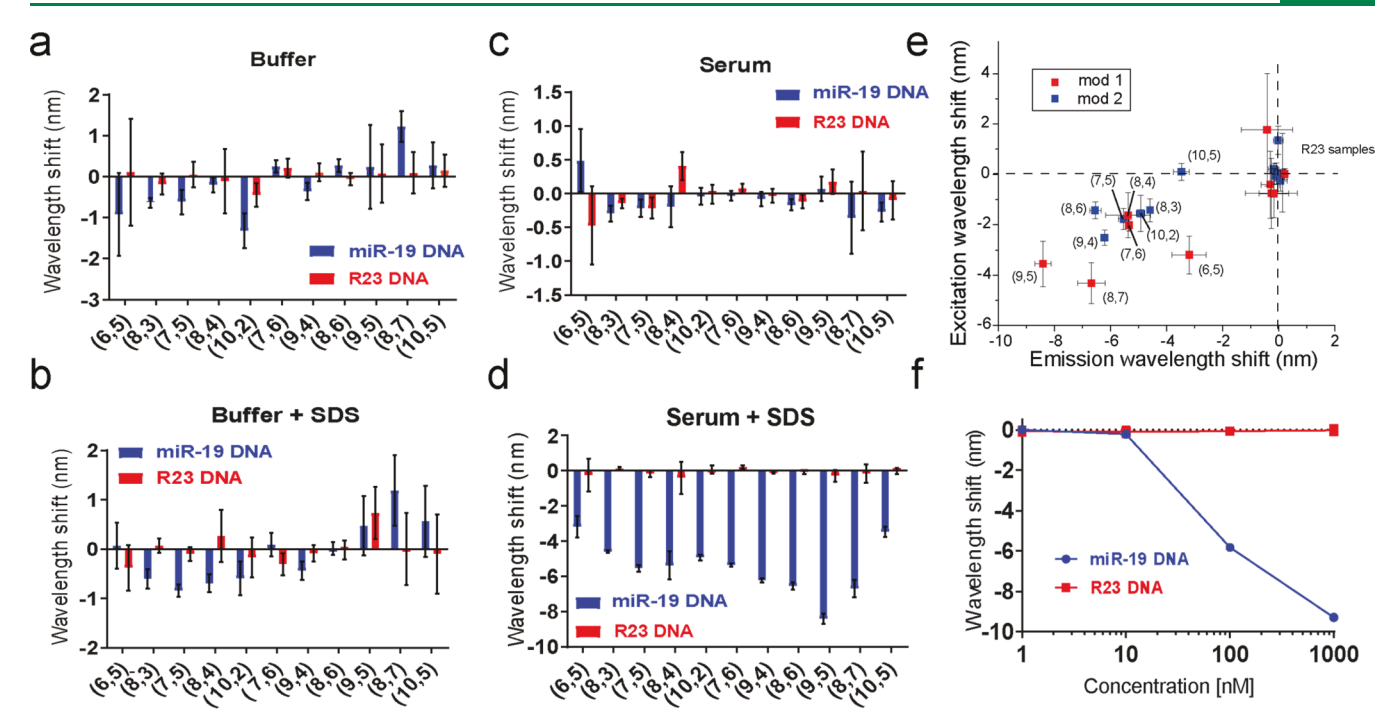


Figure 1. Modulation of the  $GT_{15}$ miR19 nanotube sensor response to nucleic acids. a. Wavelength shifting response of the  $GT_{15}$ miR19 nanotube sensor after overnight incubation with 1  $\mu$ M target miR-19 DNA (blue) or control R23 DNA (red) for the indicated nanotube chiralities in buffer. b. Wavelength shift after overnight incubation with 1  $\mu$ M target miR-19 DNA (blue) or control R23 DNA (red) for the indicated nanotube chiralities in 1% SDS. c. Wavelength shift of the  $GT_{15}$ miR19 nanotube sensor after overnight incubation with 1  $\mu$ M target miR-19 DNA (blue) or control R23 DNA (red) for the indicated nanotube chiralities in fetal bovine serum (FBS). d. Wavelength shift after overnight incubation with 1  $\mu$ M miR-19 target DNA (blue) or control R23 DNA (red) for the indicated nanotube chiralities in FBS treated with 1% SDS. e. Plots of excitation and emission wavelength shift in response to target miR-19 DNA and control R23 DNA in serum treated with 1% SDS. Nanotubes treated with target DNA are labeled by chirality, while the labels for nanotubes treated with R23 control DNA labels were omitted for clarity. Colors indicate mod type of the nanotube. Error bars represent standard deviation of technical triplicates. f. Wavelength shift of  $GT_{15}$ miR19 nanotube sensor after overnight incubation with indicated concentrations of target miR-19 DNA (blue) or control R23 DNA (red) in FBS treated with 1% SDS. Error bars represent standard deviation of technical replicates.

modulation of their intrinsic photoluminescence. <sup>10</sup> Carbon nanotubes are fluorescent in the near-infrared range<sup>11</sup> and are highly resistant to photobleaching. <sup>12</sup> Many nanotube species (chiralities) are available and defined in part by unique excitation and emission bands. <sup>13</sup> Carbon nanotube emission responds to changes in the local dielectric environment, <sup>14–16</sup> including changes in local static charge. <sup>17,18</sup>

Carbon nanotubes were recently used to detect biomarker oligonucleotides such as microRNA directly in biological fluids such as serum and urine. While such carbon nanotube sensors were shown to detect target oligonucleotides in simple buffer conditions with a modest shift in emission wavelength, the optical change upon detection was enhanced by the presence of the surfactant sodium dodecylbenzenesulfonate (SDBS). This was mediated by changes in the nanotube surface coverage of the DNA upon hybridization, resulting in increased binding of SDBS to the nanotube surface, inducing changes in the optical bandgap. The enhancement effect was found to persist in biofluids such as serum and urine and enabled detection of short DNA oligonucleotides and microRNA. 19

Herein, we describe the optical detection of HIV in complex media by a carbon nanotube sensor. Intact viruses and protein-rich solutions such as serum normally prevent detection of target viral oligonucleotides. We found that, in the presence of serum, a denaturing surfactant mediated enhanced nanotube emission response to viruses. To deduce the mechanism of this enhancement, purified proteins such as bovine serum albumin,

 $\gamma$ -globulins, casein, and hydrolyzed casein peptides were assessed. We conclude that hydrophobic pockets of surfactant-denatured protein interact with the nanotube upon hybridization, leading to a greatly enhanced blue-shift. We assessed the potential for clinical application by measuring single-strand viral RNA from an intact HIV using the nanotube sensor, resulting in successful detection. This work portends the use of carbon nanotubes for point-of-care optical detection of viruses via measurement of viral nucleic acids.

#### ■ RESULTS AND DISCUSSION

Using a carbon nanotube-based sensor for the miR-19 microRNA sequence (GT<sub>15</sub>miR19) as previously described, <sup>19</sup> we characterized the effect of serum proteins on the nanotube response using a single-stranded miR-19 DNA analyte sequence. In buffer-only conditions, the target, miR-19 DNA, produced a blue-shift in nanotube emission for most nanotube species (chiralities). However, the addition of fetal bovine serum (FBS, 10%), abrogated wavelength changes in response to the target oligonucleotide (Figure S1a). Two-dimensional photoluminescence excitation/emission (PLE) spectroscopy was used to assay optical changes for 11 different nanotube chiralities incubated with FBS after addition of the target miR-19 oligonucleotide or a noncomplementary R23 DNA control strand (Figure S3). For every chirality measured, FBS abrogated optical changes in response to the target oligonucleotide (Figure 1a-c). To better understand the effect of FBS on the sensor baseline fluorescence, we measured the

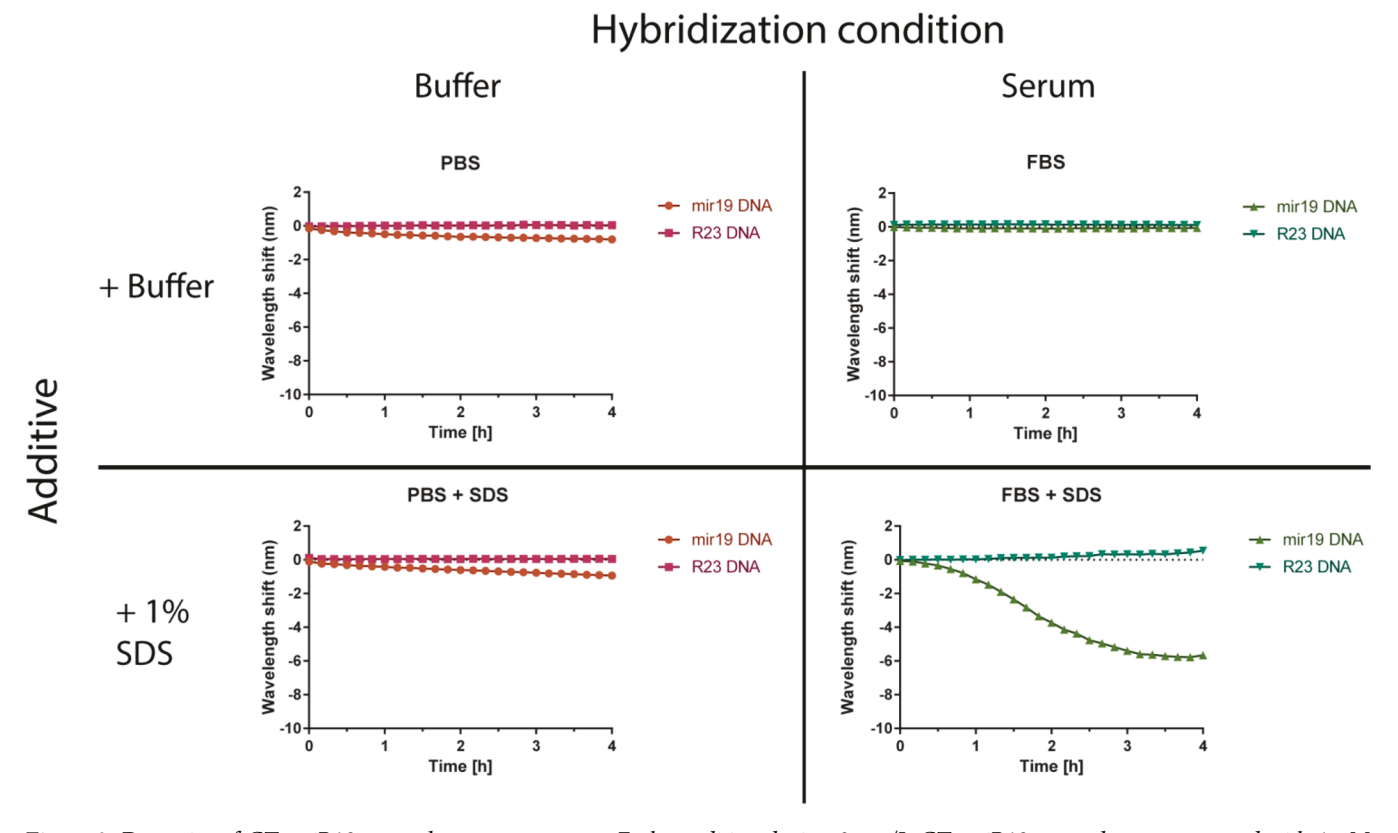


Figure 2. Dynamics of  $GT_{15}$ miR19 nanotube sensor response. Each condition depicts 2 mg/L  $GT_{15}$ miR19 nanotube sensor treated with 1  $\mu$ M target miR-19 DNA (orange in PBS, light green in serum) or control R23 DNA (purple in PBS, dark green in serum) added at time 0.

optical changes of the sensor as a function of FBS concentration in the absence of miR-19 DNA. Increasing concentrations of FBS induced red-shifting and a comcomitant increase in intensity (Figure S1b,c). Because nanotube emission responds to changes in the local dielectric environment, we interpret these red-shifting and intensity responses as resulting from proteins in the serum closely associating with the bare-regions of the DNA coated nanotubes, electrostatically interacting with the phosphate backbone to induce DNA conformation changes, or some combination thereof.

In an attempt to reduce this apparent FBS-induced fouling of the sensor, we hypothesized that an anionic detergent, sodium dodecyl sulfate (SDS), may associate with bare regions of the nanotube and block nonspecific binding of serum components. We base this hypothesis on previous works showing that SDS can be used to suspend carbon nanotubes, due to hydrophobic interactions between the nanotube surface and the 12-carbon-long alkyl chain.<sup>20</sup> We first tested whether SDS would change the baseline emission of the GT<sub>15</sub>miR19 sensor. Dilutions ranging from 0.1% to 1 wt %/vol SDS showed no significant changes in emission wavelength (Figure S2a) or intensity (Figure S2b). When hybridization of target DNA was measured in the presence of SDS via PLE spectroscopy (Figure S3), only a slight enhancement was observed for some chiralities, compared to the buffer-only condition (Figure 1b). Although SDS seemed to have little effect on the DNA-wrapped nanotube baseline fluorescence and changes during hybridization, we hypothesized that SDS may preserve the response to hybridization under serum conditions. The GT<sub>15</sub>miR19 sensor was then added to whole FBS with target or control oligonucleotide, followed by addition of concentrated SDS to a final concentration of 1%.

After 4 h, PLE plots were acquired to measure the nanotube optical response (Figure S3). Surprisingly, all observed nanotube species showed a greatly enhanced solvatochromic response to target oligonucleotide, with emission blue-shifting from 3 to 9 nm depending on chirality (Figure 1d). The excitation wavelengths ( $E_{22}$ ) also shifted, suggesting a change in the ground-state absorption (Figure 1e). When the concentration of miR-19 DNA was varied, the sensor retained dose-dependent blue-shifting behavior (Figure 1f).

We next measured the kinetics of the sensor response. The nanotube emission response was measured upon introduction of target miR-19 DNA and noncomplementary control R23 DNA in both PBS buffer and serum, with and without SDS (Figure 2). Addition of SDS to buffer-only conditions had little effect as compared to the buffer control, and there was also no response in untreated serum. The combination of serum and SDS produced a greatly enhanced blue-shift within approximately 30 min. Compared to the buffer conditions, the shape of the kinetic trace was sigmoidal with an inflection point around 2 h that reached a minimum by 3 h. In the FBS conditions with SDS, there was a slight red-shift of the sensor in response to the R23 control DNA strand. This is likely because of the nonspecific adsorption of the denatured protein to the baseline amount of exposed nanotube surface. It is probable that it is more apparent in the presence of SDS over the FBS alone because denaturing the protein structure exposes additional hydrophobic patches that become available for binding. The nonspecific FBS induced red-shifting of DNAwrapped nanotubes was discussed above (Figure S1).

We assessed the effect of surfactants on the sensor kinetics in both buffer and serum conditions. We previously reported hybridization-induced enhancement of solvatochromic changes

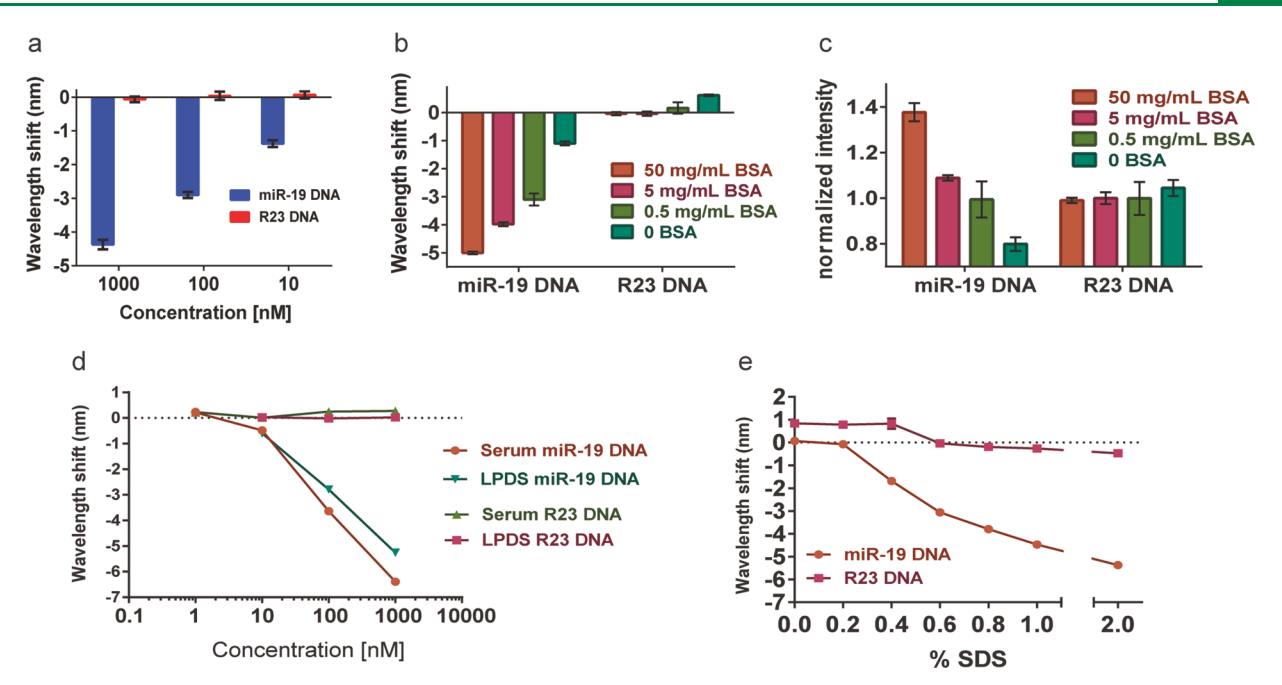


Figure 3.  $GT_{15}$ miR19 nanotube sensor response to albumin. a. Shifting of the (9,4) nanotube emission wavelength after treatment of the  $GT_{15}$ miR19 nanotube sensor with the indicated concentration of target or control DNA in 50 mg/mL BSA treated with 1% SDS. b. Wavelength shift after treatment with 1  $\mu$ M target miR-19 DNA or control R23 DNA in PBS with 1% SDS and the indicated concentration of bovine serum albumin (BSA). c. Intensity changes of  $GT_{15}$ miR19 nanotube sensor after treatment with 1  $\mu$ M miR-19 target DNA or control R23 DNA in PBS with 1% SDS and the indicated concentration of BSA. d. Wavelength shifting response of  $GT_{15}$ miR19 to dilutions of target miR-19 DNA or control R23 DNA in fetal bovine serum (FBS) treated with 1% SDS or human lipoprotein-deficient serum treated with 1% SDS after incubation overnight. e. Wavelength shifting response after overnight incubation with 50 mg/mL BSA and 1  $\mu$ M of target miR-19 (orange) or control R23 (purple) DNA and escalating concentrations of SDS. All error bars represent standard deviation.

using sodium dodecylbenzenesulfonate (SDBS), which also enabled detection in serum conditions. 19 The presence of SDBS produced a similar line shape regardless of buffer or serum conditions and resulted in a blue-shifting response that exhibited pseudo-first-order kinetics (Figure S4a). The similar response in buffer and serum suggests the same mechanism in both conditions, wherein SDBS interacts with newly exposed regions of the nanotube upon hybridization of the bound DNA. In the presence of SDS in serum, upon the introduction of DNA, there was a lag period before an optical blue-shifting (Figure S4b). Although slower than SDBS, the SDS + serum combination produced a final blue-shifted value of greater magnitude (Figure S4c,d). Because SDS minimally enhanced the wavelength shifting in the absence of serum, and because of the relatively complex kinetics of SDS + serum enhancement compared to SDBS, we hypothesized that SDS-denatured a protein component of the serum that subsequently bound to the newly exposed regions of the nanotube upon hybridization, to provide an enhanced blue-shifting response.

We tested the hypothesis that albumin, one of the most abundant macromolecules in serum, elicits the enhanced hybridization response in the presence of SDS. Serum albumin ranges from 35 mg/mL to 50 mg/mL in healthy individuals. Using purified bovine serum albumin (BSA), we tested the high end of the normal range, 50 mg/mL, with SDS to determine if this purified component of serum would enhance the nanotube response to hybridization in the absence of other serum components. A serial dilution of miR-19 DNA produced dose-dependent enhanced blue-shifting, suggesting that BSA + SDS elicited enhancement of the emission wavelength response upon hybridization (Figure 3a). We next kept the concentration of target DNA and SDS constant at 1  $\mu$ M and

varied the concentration of BSA. For most chiralities, there was a BSA dose-dependent pattern in blue-shifting and intensity enhancement (Figure 3b,c). Although some chiralities exhibited less wavelength shifting at the highest protein concentration, interestingly, even in these cases, the intensity enhancement was still dose-dependent. (Figure S5).

Serum is a complex biological fluid with many protein and nonprotein components. Because nonpolar compounds tend to cause blue-shifting of nanotube emission,  $^{23,24}$  we hypothesized that lipoproteins, which transport nonpolar fats, may be the component of serum responsible for SDS-induced hybridization enhancement.  $\rm GT_{15}miR19$  sensor was spiked into human lipoprotein-deficient serum (LPDS) or standard FBS with different concentrations of target DNA, followed by addition of concentrated SDS to a final concentration of 1 wt %/vol. The dose—response behavior and magnitude of blue-shift upon hybridization with target oligonucleotide was largely indistinguishable between the two serum conditions (Figure 3d), suggesting that lipoproteins do not play a role in the BSA-mediated response.

Finally, we kept the concentration of BSA and target oligonucleotide constant and varied the SDS concentration. We escalated the concentration from 0% to 6% in 1% increments, but observed no additional enhancement above 2% SDS (Figure 3e). Narrowing the tested concentrations between 0% and 1% in 0.1% increments revealed, however, that blue-shifting was dose-dependent in this range. This response is in accordance with reports of SDS-mediated BSA denaturation. This change occurs in the proximity of the critical micelle concentration (CMC) of SDS, which is approximately 0.23% wt/vol. These data support our hypothesis that SDS-denatured protein is a major causative

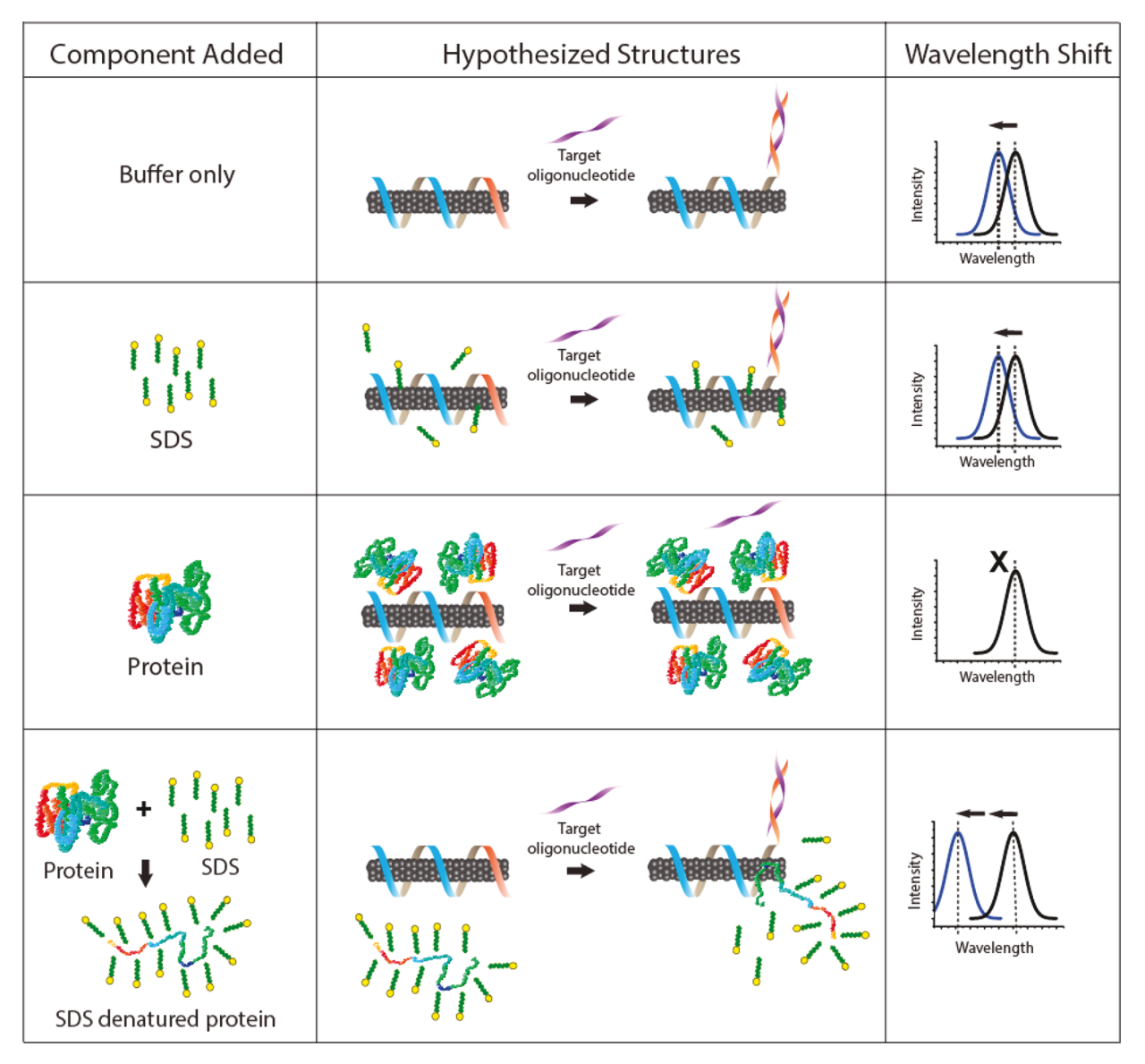


Figure 4. Summary of  $GT_{15}$ miR19 nanotube sensor responses and models of hypothesized interactions. Gray cylinders represent the carbon nanotube, and suspending DNA is represented by blue ( $GT_{15}$  portion) and orange (complementary region to target oligonucleotide) ribbon.

agent in serum for the observed hybridization-induced enhancement of the blue-shifting response of the nanotubes.

Considerable effort has been made toward understanding the microstructure and mechanism of SDS denaturation of proteins, including the relative contribution of hydrophobic interactions versus ionic interactions.<sup>27–29</sup> The currently accepted view is that below the critical micelle concentration of SDS, protein tertiary structure unfolds,<sup>30</sup> and at micellar concentrations, chain expansion drives complete denaturation. The interaction is predominantly hydrophobic at submicellar concentrations, and exclusively hydrophobic at micellar concentrations. In this model, the chain expansion is driven by micelle nucleation on hydrophobic patches of the protein chain.<sup>31</sup> In other words, increasing concentrations of SDS increase the fraction of denatured protein, which becomes available to adsorb onto the exposed surface of the nanotube. The probability of a protein denaturing in the presence of SDS depends on its aggregation state. That is, as a monomer, detergents bind to the native protein as a conventional ligand would, in a fixed number of possible binding sites. As the

concentration of detergent increases, it begins to form micelles, which are denaturing to the surrounding proteins. Therefore, global protein unfolding typically occurs above the micelle-forming concentration, or critical micellar concentration (CMC).<sup>32</sup> For SDS specifically, this occurs at 7 mM, or 0.23 wt %/vol in water, as mentioned above. Since we see no additional change above 2% SDS, we believe the enhancement effect is saturable, and thus dependent on the denaturation status of the proteins in the system. Below the CMC, the concentration of SDS directly affects the amount of denatured proteins; therefore it affects the magnitude of the shift.

Based on our experimental observations and this model, we propose the following mechanism for SDS-denatured protein enhancement of hybridization-induced blue-shifting: hybridization with miR-19 oligonucleotide leads to partial desorption of DNA from the nanotube, exposing the hydrophobic surface to the solvent conditions. SDS drives the loss of tertiary structure and exposure of hydrophobic patches on the polypeptide chain, which would typically be coated by an SDS micelle, have a stronger affinity for the newly exposed

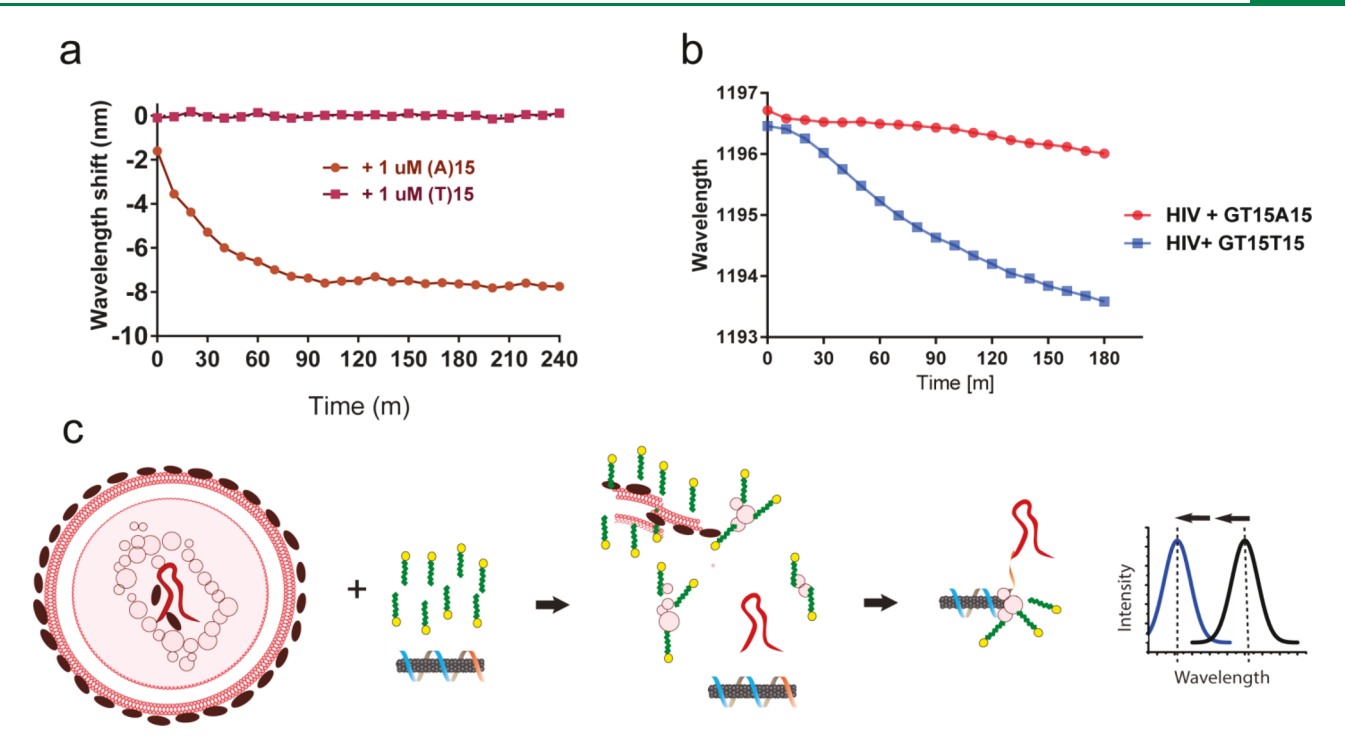


Figure 5. Detection of intact virus RNA using a HIV lentivirus model. a. Kinetics of wavelength shift of nanotube suspended with the DNA oligonucleotide  $(GT)_{15}$ - $(T)_{15}$ , focusing on the (8,6) nanotube species, upon introducing target oligonucleotide,  $(A)_{15}$ , or nontarget control,  $(T)_{15}$ , with 0.2% SDBS. b. Kinetics of the response of  $(GT)_{15}$ - $(T)_{15}$  or  $(GT)_{15}$ - $(A)_{15}$ -suspended nanotubes with concentrated HIV and 2% SDS. c. Model depicting HIV RNA detection. The virus is ruptured and denatured by SDS, liberating the RNA genome, which hybridizes to the sensor, freeing space on the nanotube surface. Denatured viral proteins bind to the freed space on the nanotube surface, eliciting an enhanced blue-shifting response.

nanotube surface than with SDS, leading to preferential binding of the hydrophobic patch to the nanotube surface.

The competition between SDS and the bare nanotube surface for the hydrophobic patch may explain the relatively slow kinetics compared to SDBS (Figure S4). The proteinnanotube interaction is expected to decrease the local dielectric environment around the nanotube, producing the observed blue-shift in emission. The remainder of the DNA-coated nanotube is protected due to charge-charge repulsion between the negatively charged SDS-denatured protein chain and the negatively charged DNA phosphate backbone. Because SDS does not change baseline fluorescence of the nanotube (Figure S3) and produces almost no enhancement of blueshifting after hybridization with the target in the absence of protein (Figure 1b), we conclude that free SDS alone makes little contribution to the observed blue-shift. Protein alone results in red-shifting of the nanotube emission and largely prevents hybridization (Figure 1a, Figure S1a), possibly due to electrostatic interactions with the DNA-suspended nanotube 19 that are eliminated by SDS coating the protein chain. The hybridization conditions and resulting optical outputs are summarized in Figure 4.

We next investigated the impact of the protein size and tertiary character on SDS-denatured protein enhancement of hybridization-induced blue-shifting. Using the relatively large  $\gamma$ -globulins (1200 kDa compared to albumin, 66.5 kDa), a subset of the second most abundant protein class in serum after albumin, we tested if SDS-mediated denaturation would lead to enhanced blue-shifting upon hybridization. A solution of  $\gamma$ -globulins at 35 mg/mL was exposed to 2 wt %/vol SDS with target or control DNA. In this case, although we found that the sensor response to SDS-denatured  $\gamma$ -globulins was

relatively slow, there was a similar equilibrium of blue-shifting compared to BSA (Figure S6a). Unlike BSA, SDS-denatured  $\gamma$ -globulins did not lead to increased emission intensity upon hybridization (Figure S6c).

We also examined another protein, casein, the main protein component of milk, which is not found in serum but has a micellar tertiary structure as a distinguishing characteristic.<sup>34</sup> Hydrolyzed casein, which is casein that has been digested into smaller peptide and protein fragments, was also tested to compare the effect of protein fragmentation. We tested whether SDS + casein would recapitulate the results seen for BSA and immunoglobulins, and whether SDS + hydrolyzed casein would produce any enhancement due to the fragmentation from partial digestion. Casein and hydrolyzed casein were prepared at 35 mg/mL and SDS was added to 2 wt %/vol, followed by target or control DNA. For most chiralities, SDS + casein enhanced hybridization-induced blue-shifting and intensity increases, while hydrolyzed casein elicited only modest enhancement over controls (Figure S6b,d). This is consistent with work showing that the degree of hydrolysis of casein is correlated with loss of hydrophobicity.<sup>35</sup> However, we noted that some chiralities showed significant hybridizationinduced blue-shifting enhancement with SDS + hydrolyzed casein, sometimes exceeding the enhancement produced by SDS + casein (Figure S6e-h). These results suggest that most proteins, independent of their tertiary structure, combined with SDS, will lead to hybridization-induced enhancement with a similar magnitude at equilibrium. A relatively long protein chain appears to be important, as most chiralities did not respond well to SDS + hydrolyzed casein as an enhancing agent. Two nanotube chiralities were notable exceptions, where SDS + hydrolyzed casein performed better than full

length casein. Chirality-dependent selectivity to analytes has been reported <sup>19,36,37</sup> but the mechanism for chirality selectivity observed here requires further study.

We examined whether the single-stranded RNA genome<sup>38</sup> of intact HIV particles could be detected by the sensor via denatured protein-mediated enhancement. We hypothesized that SDS could be both applied to liberate the genome of the viruses and additionally to denature proteins for hybridizationinduced enhancement of the sensor. A sensor was constructed to hybridize to the polyadenylation elements of HIV RNAs by using the DNA oligonucleotide sequence  $(GT)_{15}$ - $(T)_{15}$  DNA to suspend carbon nanotubes. As a control, a sensor for a polyuridine or polythymine sequences, which are not known to exist in HIV, was similarly constructed with the sequence (GT)<sub>15</sub>-(A)<sub>15</sub> DNA. The function of both sensors was first assessed with short strands of target DNA and 0.2% SDBS, based on the assumption that DNA would hybridize to the sensor as well as RNA.<sup>39</sup> The sensor for poly-A sequences, (GT)<sub>15</sub>-(T)<sub>15</sub>, showed a rapid (complete in 90 min) and robust blue-shift when treated with (A)<sub>15</sub>, but no change was observed after treatment with (T)15, which served as a control for nonspecific oligonucleotide binding (Figure 5a).

To test the sensor with intact HIV particles, we used established methods for production of recombinant HIV particles engineered to be replication-incompetent for safety. 40 Suspensions of viral particles were treated with 1% SDS and  $(GT)_{15}$ - $(T)_{15}$  in FBS, the sensor for the poly(A) elements, or with  $(GT)_{15}$ - $(A)_{15}$ , to serve as a negative control. The center wavelength of the (8,6) nanotube was measured every 10 min over 180 min. The sensor for poly(A) sequences, (GT)<sub>15</sub>- $(T)_{15}$ , began to blue-shift within 20 min, and by 180 min had shifted about 3 nm. The kinetics exhibited a sigmoidal shape, suggesting enhancement from denatured viral proteins. The control sensor, (GT)<sub>15</sub>-(A)<sub>15</sub>, blue-shifted by about 0.5 nm over 180 min, indicating presumably nonspecific interactions (Figure 5b). We present a model for such detection, illustrated in Figure 5c. Here, intact HIV is treated with SDS and a carbon nanotube sensor. The SDS denatures the HIV envelope and protein structure, releasing the single-strand RNA genome. Hybridization with the poly A tail enables binding by the detergent-denatured protein, leading to a blue-shift of the nanotube emission.

### CONCLUSIONS

Here, we investigated the detection of HIV by carbon nanotube photoluminescence. We found that SDS-treated serum can interact with carbon nanotubes to enhance the blueshifting response of hybridization-induced removal of DNA from the nanotube surface. In understanding why SDS-treated serum provided such enhancement, we examined lipoproteindeficient serum as well as purified serum proteins to identify the causative agent. We found that purified albumin, in the presence of SDS, could largely, but not totally, recapitulate the enhancement seen with serum. We surmise that the other proteins in serum may elicit the larger response, although it is conceivable that nonprotein factors could be responsible.<sup>22</sup> The enhancement to hybridization-induced blue-shifting by SDS-treated protein was unexpected due to the fact that SDS alone does very little to DNA-suspended nanotubes, and protein alone results in red-shifting of DNA-suspended nanotubes. Based on the current understanding of SDSinduced protein denaturation and the mechanism of the DNAcarbon nanotube sensor, we propose a model where hydrophobic residues from the SDS-denatured protein bind to newly exposed nanotube surface after hybridization of the DNA on the nanotube, leading to the enhancement in blue-shifting.

For clinical applications, we believe that diagnostics based on detection of viruses in protein rich environments such as serum could benefit from a rapid optical sensor. We previously reported in vivo and serum measurements using another detergent, SDBS, to enhance detection of oligonucleotides. In serum, we believe that SDBS and SDS operate with two distinct mechanisms, where SDBS interacts with the nanotube directly after hybridization, while SDS functions to expose hydrophobic centers in denatured proteins, which then interacts with the nanotube. Although SDBS produces a faster response in serum, SDS produces a shift with a greater magnitude.

As a proof-of-principle for direct optical detection of a virus in vitro, we showed how SDS can be combined with a DNAnanotube sensor to both liberate lentiviral RNA from a complete virus structure and elicit an enhanced response to the analyte RNA via binding of SDS-denatured viral proteins to the space liberated on the nanotube by the hybridization event. The shifting response in the presence of intact HIV (Figure 5b), however, was less robust than the same sequence of DNA (Figure 5a). In the initial development of the sensor construct, a similar phenomenon was noted. 19 The hybridization of RNA to the sensor was noticed to be consistently slower than the same sequence of DNA and it often continued to trend downward, even after 180 min. This was attributed to the longer persistence length and higher rigidity of single-stranded RNA compared to single-stranded DNA. In Figure 5b, the difference at 180 min is distinct enough for the purposes of an in vitro sensor; therefore, the experiment was terminated at this time point. Because the kinetics are similar to the wellestablished response of the sensor to RNA, and because of the investigation of different protein responses in Figure S6, we are confident that the sensor is responding to the viral RNA specifically.

Such methods could take place directly in serum samples where point-of-care detection is desirable. Field applications in low-resource settings are also possible, as the DNA—nanotube sensor solution and SDS are both highly stable and can be stored at room temperature. In addition, an inexpensive and robust detection device could be developed using standard photodetectors and LED light sources for deployment in regions lacking critical biomedical infrastructure. Many viruses of interest, such as Ebola, are viruses with single-stranded RNA genomes that may be amenable to detection with this method. While we have shown here an application with a lentivirus model, we believe that SDS could also be applied to detection of single-strand oligonucleotides in other viruses and pathogen types, as well as in circulating cancer cells.

## ■ MATERIALS AND METHODS

(Coralville, IA). Following ultrasonication, the dispersions were ultracentrifuged (Sorvall Discovery 90SE) for 30 min at 280,000g and the top 80% of the supernatant was collected. Absorbance spectra were acquired using a UV/vis/nIR spectrophotometer (Jasco V-670, Tokyo, Japan). The concentration for HiPco samples was calculated using the extinction coefficient Abs<sub>910</sub> = 0.02554 L mg<sup>-1</sup> cm<sup>-1</sup>. Excess DNA was removed via 100 kDa Amicon centrifuge filters (Millipore). The DNA–nanotube complexes were resuspended in PBS (Thermo Fisher Scientific Waltham, MA).

**Fluorescence Spectroscopy Measurements of Carbon Nanotubes.** Fluorescence emission spectra from aqueous nanotube solutions were acquired with a home-built spectroscopy system as described. Briefly, carbon nanotube samples were assayed in a 96 well plate format on an inverted microscope using a tunable white-light laser (NKT Photonics) coupled to a variable bandpass filter. Emission light was directed into a spectrometer with a focal length of 320 mm and aperture ratio of f/4.6 (Princeton Instruments IsoPlane SCT 320) and InGaAs array camera (Princeton Instruments 640 × 512 pixel NIRvana). For all experiments, measurements were taken in triplicate across three wells. Following spectra acquisition, custom code written in Matlab applied spectral corrections and background subtraction as described. Corrected spectra were used to fit the data with Voigt functions. Error bars and linear fits were computed with GraphPad Prism 6.

Hybridization Conditions. Concentrated sodium dodecyl sulfate (Sigma-Aldrich) was prepared in PBS buffer and added to samples to the final concentration indicated, or 1 wt %/vol where not indicated; control samples had an equivalent volume of PBS added. Carbon nanotubes were used at a final concentration of 2 mg/L for all experiments. Fetal bovine serum (FBS) (Life Technologies) and human lipoprotein deficient serum (LPDS) (J65516 Lipoprotein Deficient Serum, human, BT-931 from Alfa Aesar) were used for serum-based experiments, and had concentrated nanotubes or SDS added directly to the whole serum. Bovine serum albumin, bovine  $\gamma$ globulins, casein, and hydrolyzed casein (all from Sigma-Aldrich) were resuspended in PBS to the indicated concentrations. Concentrated target DNA (TGTGCAAAATCTATGCAAAACTGA) complementary to the DNA-nanotube sensor or noncomplementary control DNA (TCGGTCAGTGGGTCATTGCTAGT) (both from IDT DNA, Coralville, IA) was added to the indicated final concentration. Nontreated controls received an equivalent volume of PBS. Hybridization was allowed to proceed overnight for equilibrium measurements. Kinetics were measured immediately after addition of target. Assessment of (GT)<sub>15</sub>-(T)<sub>15</sub> and (GT)<sub>15</sub>-(A)<sub>15</sub> used 0.2% SDBS (Sigma-Aldrich) as described<sup>19</sup> to verify expected behavior with AAAAAAAAAAAAA or TTTTTTTT-TTTTTTT (IDT DNA, Coralville, IA).

HIV Production. Lentivirus HIV was produced from transfected packaging cells (293T) using 100 ng pLX304 plasmid, <sup>38</sup> 100 ng of packaging plasmid (psPAX2) and 10 ng of envelope plasmid (VSV-G). Virus was collected 48 and 70 h after transfection and concentrated 10-fold.

#### ASSOCIATED CONTENT

#### S Supporting Information

The Supporting Information is available free of charge on the ACS Publications website at DOI: 10.1021/acssensors.9b00025.

Impact of serum on  $GT_{15}$ miR19 nanotube sensor function; Baseline effects of SDS on the  $GT_{15}$ miR19 nanotube sensor; Modulation of the  $GT_{15}$ miR19 nanotube sensor response in the presence of serum with and without SDS; Kinetics of surfactant-mediated  $GT_{15}$ miR19 nanotube sensor response; Chirality-specific behavior of the  $GT_{15}$ miR19 sensor response to hybridization mediated by BSA + SDS; Effects of proteins and protein structure on  $GT_{15}$ miR19 nanotube sensor response (PDF)

#### AUTHOR INFORMATION

#### **Corresponding Author**

\*E-mail: hellerd@mskcc.org.

ORCID ®

Jackson D. Harvey: 0000-0001-8700-0713 Hanan A. Baker: 0000-0001-6305-5875 Daniel A. Heller: 0000-0002-6866-0000

#### **Notes**

The authors declare the following competing financial interest(s): D.H. and J.H. are named on a patent application filed by MSKCC related to this work (application no. WO2017177131A1, title: Sensors for nucleic acid biomarkers). The following disclosures are unrelated to this work: D.H. is a cofounder of LipidSense, Inc. and is a cofounder and officer with equity interest in Goldilocks Therapeutics Inc., as well as a member of the scientific advisory board of Oncorus, Inc. H.A.B is a cofounder of Pictesque Inc. A.K. serves as a consultant for Novartis.

#### ACKNOWLEDGMENTS

This work was supported in part by the NIH New Innovator Award (DP2-HD075698), the Cancer Center Support Grant (P30 CA008748), the National Science Foundation CAREER Award (1752506), the American Cancer Society Research Scholar Grant (GC230452), the Pershing Square Sohn Cancer Research Alliance, the Honorable Tina Brozman Foundation for Ovarian Cancer Research, the Expect Miracles Foundation - Financial Services Against Cancer, the Anna Fuller Fund, the Louis V. Gerstner Jr. Young Investigator's Fund, the Frank A. Howard Scholars Program, Cycle for Survival, the Alan and Sandra Gerry Metastasis Research Initiative, Mr. William H. Goodwin and Mrs. Alice Goodwin and the Commonwealth Foundation for Cancer Research, the Experimental Therapeutics Center, the Imaging & Radiation Sciences Program, and the Center for Molecular Imaging and Nanotechnology of Memorial Sloan Kettering Cancer. M.O. is supported by the Family and Friends of Caroline Bhatt, Met Life Foundation, and the National Cancer Institute (#K12CA184746). H.A.B. was supported by a Medical Scientist Training Program grant from the National Institute of General Medical Sciences of the NIH under award number T32GM007739 to the Weill Cornell/Rockefeller/Sloan-Kettering Tri-Institutional MD-PhD Program. A.K. is the Damon Runyon-Richard Lumsden Foundation Clinical Investigator, and acknowledges support from the St. Baldrick's Foundation Robert J. Arceci Innovation Award.

## **■** REFERENCES

- (1) Schito, M. L.; D'Souza, M. P.; Owen, S. M.; Busch, M. P. Challenges for rapid molecular HIV diagnostics. *J. Infect. Dis.* **2010**, 201, S1–6.
- (2) Schwarzenbach, H.; Hoon, D. S.; Pantel, K. Cell-free nucleic acids as biomarkers in cancer patients. *Nat. Rev. Cancer* **2011**, *11* (6), 426.
- (3) Mitchell, P. S.; Parkin, R. K.; Kroh, E. M.; Fritz, B. R.; Wyman, S. K.; Pogosova-Agadjanyan, E. L.; Peterson, A.; Noteboom, J.; O'Briant, K. C.; Allen, A.; et al. Circulating microRNAs as stable blood-based markers for cancer detection. *Proc. Natl. Acad. Sci. U. S. A.* **2008**, *105* (30), 10513–10518.
- (4) Zen, K.; Zhang, C. Y. Circulating microRNAs: a novel class of biomarkers to diagnose and monitor human cancers. *Med. Res. Rev.* **2012**, 32 (2), 326–348.

(5) Crowley, E.; Di Nicolantonio, F.; Loupakis, F.; Bardelli, A. Liquid biopsy: monitoring cancer-genetics in the blood. *Nat. Rev. Clin. Oncol.* **2013**, *10* (8), 472.

- (6) Corsten, M. F.; Dennert, R.; Jochems, S.; Kuznetsova, T.; Devaux, Y.; Hofstra, L.; Wagner, D. R.; Staessen, J. A.; Heymans, S.; Schroen, B. Circulating MicroRNA-208b and MicroRNA-499 reflect myocardial damage in cardiovascular disease. *Circ.: Cardiovasc. Genet.* **2010**, *3* (6), 499–506.
- (7) Elnifro, E. M.; Ashshi, A. M.; Cooper, R. J.; Klapper, P. E. Multiplex PCR: optimization and application in diagnostic virology. *Clin. Microbiol. Rev.* **2000**, *13* (4), 559–570.
- (8) Niemz, A.; Ferguson, T. M.; Boyle, D. S. Point-of-care nucleic acid testing for infectious diseases. *Trends Biotechnol.* **2011**, 29 (5), 240–250.
- (9) Huang, X.; Liu, Y.; Yung, B.; Xiong, Y.; Chen, X. Nanotechnology-enhanced no-wash biosensors for in vitro diagnostics of cancer. ACS Nano 2017, 11 (6), 5238–5292.
- (10) Kruss, S.; Hilmer, A. J.; Zhang, J.; Reuel, N. F.; Mu, B.; Strano, M. S. Carbon nanotubes as optical biomedical sensors. *Adv. Drug Delivery Rev.* **2013**, *65* (15), 1933–1950.
- (11) O'connell, M. J.; Bachilo, S. M.; Huffman, C. B.; Moore, V. C.; Strano, M. S.; Haroz, E. H.; Rialon, K. L.; Boul, P. J.; Noon, W. H.; Kittrell, C. Band gap fluorescence from individual single-walled carbon nanotubes. *Science (Washington, DC, U. S.)* **2002**, 297 (5581), 593–596.
- (12) Wang, F.; Dukovic, G.; Brus, L. E.; Heinz, T. F. The optical resonances in carbon nanotubes arise from excitons. *Science (Washington, DC, U. S.)* **2005**, 308 (5723), 838–841.
- (13) Roxbury, D.; Jena, P. V.; Williams, R. M.; Enyedi, B.; Niethammer, P.; Marcet, S.; Verhaegen, M.; Blais-Ouellette, S.; Heller, D. A. Hyperspectral microscopy of near-infrared fluorescence enables 17-chirality carbon nanotube imaging. *Sci. Rep.* **2015**, *5*, 14167.
- (14) Heller, D. A.; Pratt, G. W.; Zhang, J.; Nair, N.; Hansborough, A. J.; Boghossian, A. A.; Reuel, N. F.; Barone, P. W.; Strano, M. S. Peptide secondary structure modulates single-walled carbon nanotube fluorescence as a chaperone sensor for nitroaromatics. *Proc. Natl. Acad. Sci. U. S. A.* **2011**, *108* (21), 8544–8549.
- (15) Heller, D. A.; Jeng, E. S.; Yeung, T.-K.; Martinez, B. M.; Moll, A. E.; Gastala, J. B.; Strano, M. S. Optical detection of DNA conformational polymorphism on single-walled carbon nanotubes. *Science (Washington, DC, U. S.)* **2006**, *311* (5760), 508–511.
- (16) Jena, P. V.; Roxbury, D.; Galassi, T. V.; Akkari, L.; Horoszko, C. P.; Iaea, D. B.; Budhathoki-Uprety, J.; Pipalia, N.; Haka, A. S.; Harvey, J. D.; et al. A carbon nanotube optical reporter maps endolysosomal lipid flux. *ACS Nano* **2017**, *11* (11), 10689–10703.
- (17) Roxbury, D.; Jena, P. V.; Shamay, Y.; Horoszko, C. P.; Heller, D. A. Cell membrane proteins modulate the carbon nanotube optical bandgap via surface charge accumulation. *ACS Nano* **2016**, *10* (1), 499–506.
- (18) Budhathoki-Uprety, J.; Langenbacher, R. E.; Jena, P. V.; Roxbury, D.; Heller, D. A. A Carbon Nanotube Optical Sensor Reports Nuclear Entry via a Noncanonical Pathway. *ACS Nano* **2017**, *11* (4), 3875–3882.
- (19) Harvey, J. D.; Jena, P. V.; Baker, H. A.; Zerze, G. H.; Williams, R. M.; Galassi, T. V.; Roxbury, D.; Mittal, J.; Heller, D. A. A carbon nanotube reporter of microRNA hybridization events in vivo. *Nature biomedical engineering* **2017**, *1* (4), No. 0041.
- (20) Xu, J.; Mueller, R.; Hazelbaker, E.; Zhao, Y.; Bonzongo, J.-C. J.; Clar, J. G.; Vasenkov, S.; Ziegler, K. J. Strongly bound sodium dodecyl sulfate surrounding single-wall carbon nanotubes. *Langmuir* **2017**, 33 (20), 5006–5014.
- (21) Burtis, C. A.; Ashwood, E. R.; Bruns, D. E. Tietz textbook of clinical chemistry and molecular diagnostics-e-book; Elsevier Health Sciences: 2012.
- (22) Adkins, J. N.; Varnum, S. M.; Auberry, K. J.; Moore, R. J.; Angell, N. H.; Smith, R. D.; Springer, D. L.; Pounds, J. G. Toward a human blood serum proteome analysis by multidimensional

separation coupled with mass spectrometry. Mol. Cell. Proteomics 2002, 1 (12), 947–955.

- (23) Choi, J. H.; Strano, M. S. Solvatochromism in single-walled carbon nanotubes. *Appl. Phys. Lett.* **2007**, 90 (22), 223114.
- (24) Gao, J.; Gomulya, W.; Loi, M. Effect of medium dielectric constant on the physical properties of single-walled carbon nanotubes. *Chem. Phys.* **2013**, 413, 35–38.
- (25) Scanu, A.; Wisdom, C. Serum lipoproteins structure and function. *Annu. Rev. Biochem.* **1972**, 41 (1), 703–730.
- (26) Vlasova, I.; Zhuravleva, V.; Saletsky, A. Denaturation of bovine serum albumin initiated by sodium dodecyl sulfate as monitored via the intrinsic fluorescence of the protein. *Russ. J. Phys. Chem. B* **2014**, 8 (3), 385–390.
- (27) Chen, S.-H.; Teixeira, J. Structure and fractal dimension of protein-detergent complexes. *Phys. Rev. Lett.* **1986**, *57* (20), 2583.
- (28) Guo, X.; Zhao, N.; Chen, S.; Teixeira, J. Small-angle neutron scattering study of the structure of protein/detergent complexes. *Biopolymers* **1990**, 29 (2), 335–346.
- (29) Turro, N. J.; Lei, X.-G.; Ananthapadmanabhan, K.; Aronson, M. Spectroscopic probe analysis of protein-surfactant interactions: the BSA/SDS system. *Langmuir* **1995**, *11* (7), 2525–2533.
- (30) Ibel, K.; May, R. P.; Sandberg, M.; Mascher, E.; Greijer, E.; Lundahl, P. Structure of dodecyl sulfate—protein complexes at subsaturating concentrations of free detergent. *Biophys. Chem.* **1994**, *53* (1–2), 77–83.
- (31) Bhuyan, A. K. On the mechanism of SDS-induced protein denaturation. *Biopolymers* **2010**, 93 (2), 186–199.
- (32) Otzen, D. E. Protein unfolding in detergents: effect of micelle structure, ionic strength, pH, and temperature. *Biophys. J.* **2002**, 83 (4), 2219–30.
- (33) Shirahama, K.; TSUJII, K.; TAKAGI, T. Free-boundary electrophoresis of sodium dodecyl sulfate-protein polypeptide complexes with special reference to SDS-polyacrylamide gel electrophoresis. *J. Biochem.* **1974**, *75* (2), 309–319.
- (34) Swaisgood, H. E. Review and Update of Casein Chemistry1, 2. *J. Dairy Sci.* **1993**, 76 (10), 3054–3061.
- (35) Mahmoud, M. I.; MALONE, W. T.; Cordle, C. T. Enzymatic hydrolysis of casein: effect of degree of hydrolysis on antigenicity and physical properties. *J. Food Sci.* **1992**, *57* (5), 1223–1229.
- (36) O'Connell, M. J.; Eibergen, E. E.; Doorn, S. K. Chiral selectivity in the charge-transfer bleaching of single-walled carbon-nanotube spectra. *Nat. Mater.* **2005**, *4* (5), 412.
- (37) Salem, D. P.; Landry, M. P.; Bisker, G.; Ahn, J.; Kruss, S.; Strano, M. S. Chirality dependent corona phase molecular recognition of DNA-wrapped carbon nanotubes. *Carbon* **2016**, *97*, 147–153.
- (38) Tang, H.; Kuhen, K. L.; Wong-Staal, F. Lentivirus replication and regulation. *Annu. Rev. Genet.* 1999, 33 (1), 133-170.
- (39) Lesnik, E. A.; Freier, S. M. Relative thermodynamic stability of DNA, RNA, and DNA:RNA hybrid duplexes: relationship with base composition and structure. *Biochemistry* **1995**, 34 (34), 10807–15.
- (40) Sakuma, T.; Barry, M. A.; Ikeda, Y. Lentiviral vectors: basic to translational. *Biochem. J.* **2012**, 443 (3), 603–618.